

## RAMAN SPECTRA OF SILICON/GERMANIUM ALLOY THIN FILMS BASED ON POROUS SILICON

E. B. Chubenko,<sup>a,\*</sup> N. L. Grevtsov,<sup>a</sup> V. P. Bondarenko,<sup>a</sup>  
I. M. Gavrilin,<sup>b</sup> A. V. Pavlikov,<sup>b</sup> A. A. Dronov,<sup>b</sup>  
L. S. Volkova,<sup>c</sup> and S. A. Gavrilov<sup>b</sup>

UDC 535.375.5;539.216.2

*Regularities of composition changes of silicon/germanium alloy thin films formed on a single-crystalline silicon substrate by electrochemical deposition of germanium into a porous silicon matrix with subsequent rapid thermal annealing (RTA) at temperatures of 750–950°C are studied. An analysis of the samples by Raman spectroscopy showed that an increase of the RTA temperature leads to a decrease in the germanium concentration in the formed film. A decrease of the RTA duration at a given temperature makes it possible to obtain films with a higher germanium concentration and to control the composition of thin silicon/germanium alloy films formed by changing the RTA temperature and duration. The obtained results on controlling the composition of silicon/germanium alloy films can be used to create functional electronic devices, thermoelectric power converters, and optoelectronic devices.*

**Keywords:** porous silicon, germanium, silicon/germanium, electrochemical deposition, Raman spectroscopy.

**Introduction.** The elemental semiconductors silicon (Si) and germanium (Ge) belong to a group of elements in the Periodic Table that form crystal structures with a diamond-type lattice. Therefore, they can be mixed with each other in any proportion to form alloys  $\text{Si}_{1-x}\text{Ge}_x$ , where  $x$  is the mole fraction of Ge [1]. The properties of these alloys such as the bandgap and crystal lattice constant, depending on the value of  $x$ , can be rather accurately predicted according to the Vegard rule [2–4]. SiGe finds applications in fast-acting microelectronic devices and UHF-range integrated circuits [5, 6] because of the higher mobility of charge carriers and better transport properties than those of pure Si [4, 5]. In addition, it is considered a promising material for photovoltaic devices and photomultipliers and thermoelectric energy converters operating on the Seebeck effect [4, 6, 7]. SiGe possesses several advantages that increase the efficiency of thermoelectric converters. It has a very broad operating temperature range from 400 to 1000°C. In contrast to many oxide semiconductors, it can be doped with donor and acceptor impurities to produce electron and hole conductivity. It also has low thermal conductivity [4]. The lowering of the thermal conductivity and specific resistance upon doping SiGe simultaneously with the raising of the operating temperature makes it possible to fabricate highly efficient thermoelectric converters based on it. Therefore, the alloy  $\text{Si}_{0.8}\text{Ge}_{0.2}$  is considered a promising material for harvesting energy from the environment in various sectors from industrial installations to spacecraft [5].

Well-known vacuum deposition methods are used to produce SiGe, e.g., molecular-beam epitaxy, chemical vapor deposition, and magnetron sputtering [1, 5]. However, low-temperature approaches, e.g., electrochemical liquid–liquid–solid (ec-LLS) deposition of Ge followed by thermal annealing [8], can be used in addition to vacuum methods to produce SiGe. The ec-LLS method presupposes preliminary deposition onto a substrate of particles of a low-melting metal, e.g., indium, gallium, or tin [9–12]. Then, Ge is reduced on the surface of the metal particles, which act simultaneously as nucleation centers and electron sources. Direct electrochemical deposition of Ge occurs from alkaline aqueous solutions of  $\text{GeO}_2$  [13–15] or anhydrous solutions of Ge salts in organic solvents or ionic liquids [16, 17]. Electrochemical deposition of Ge was considered of little use [16] until interest in the production of nanostructures and alloys of this material for

\*To whom correspondence should be addressed.

<sup>a</sup>Belarusian State University of Informatics and Radioelectronics, Minsk, Belarus; email: eugene.chubenko@gmail.com; <sup>b</sup>National Research University of Electronic Technology — MIET, Moscow, Zelenograd, Russia; <sup>c</sup>Institute of Nanotechnology of Microelectronics, Russian Academy of Sciences, Moscow, Russia. Translated from Zhurnal Prikladnoi Spektroskopii, Vol. 89, No. 5, pp. 614–620, September–October, 2022. Original article submitted July 8, 2022. <https://doi.org/10.47612/0514-7506-2022-89-5-614-620>.

optoelectronics, photovoltaics, and energy conversion devices arose [8, 17, 18]. The polycrystalline nature of Ge films obtained by an electrochemical method did not prevent their use in these areas although the advantage of the deposition rate and simple equipment of low-temperature synthesis neutralized this drawback.

The present work demonstrated the ability to produce the alloys  $\text{Si}_{1-x}\text{Ge}_x$  by direct electrochemical deposition of Ge onto a porous Si matrix followed by rapid thermal annealing (RTA). Layers of  $\text{Si}_{1-x}\text{Ge}_x$  up to several micrometers thick could be produced by filling the pores of the porous Si. The layer composition could be controlled by varying the ratio of pore volume and Si crystallites in the porous Si layer, i.e., its porosity. The composition of the formed films had to be controlled to fabricate efficient thermoelectric converters or optoelectronic devices based on  $\text{Si}_{1-x}\text{Ge}_x$ . The present work showed that Raman spectroscopy (RS) could be used to solve this problem.

**Experimental.** Porous Si was formed via electrochemical anodization using a plate of single-crystalline Si with electron-type conductivity and specific resistance  $0.01 \Omega \cdot \text{cm}$ . The anodic treatment used a galvanostatic setup in an aqueous alcohol electrolyte with an HF (45%): $\text{H}_2\text{O}$ :*i*-PrOH component ratio of 1:3:1. A layer of porous Si  $1.5 \mu\text{m}$  thick was produced at current density  $70 \text{ mA/cm}^2$  for 30 s. The current source was a Metrohm Autolab PGSTAT302N potentiostat/galvanostat. Then, a low-porosity surface layer was removed from the surface of the obtained porous Si layer [19] via chemical replacement of Si atoms by Cu followed by its removal in  $\text{HNO}_3$  [8]. Ge was deposited electrochemically onto the porous Si matrix using a solution containing  $\text{GeO}_2$  (0.05 M),  $\text{K}_2\text{SO}_4$  (0.5 M), and succinic acid (0.1 M) at pH 6.5.

Thermal annealing of samples to synthesize the SiGe alloy used the RTA method on an RTP System AS-One 100. The annealing was performed in a stream of Ar (flow rate  $800 \text{ cm}^3/\text{min}$ ) at  $750\text{--}950^\circ\text{C}$  for 30–300 s. The heating rate was  $10^\circ\text{C/s}$ .

The morphology and elemental composition of the obtained samples were studied using scanning electron microscopy and energy-dispersive x-ray analysis (EDX) on an FEI Helios G4 CX DualBeam scanning electron microscope. A Horiba LabRAM HR-800 micro-Raman spectrometer equipped with a He–Ne laser excitation source at operating wavelength  $633 \text{ nm}$  was used to study sample using Raman spectroscopy.

**Results and Discussion.** The starting layer of porous Si obtained by anodic treatment and removal of the surface layer was  $1.2 \mu\text{m}$  thick (Fig. 1). Pores of average diameter  $50\text{--}70 \text{ nm}$  were formed as vertical walls of Si crystallites of slight roughness. Pore channels were filled with semiconductor particles after electrochemical deposition of Ge. A quasi-continuous porous layer of Ge particles  $30\text{--}40 \text{ nm}$  in size formed on the surface.

The morphology of the porous Si layer with deposited Ge changed considerably after RTA at various temperatures from  $750$  to  $950^\circ\text{C}$  (Fig. 2). The sample treated at  $750^\circ\text{C}$  changed the least. The preserved pore structure of the porous Si and melted particles, presumably Ge, were visible in the transverse chip. The crystallites of the Si skeleton of the porous Si alloyed with the Ge and the structure of the porous Si became less distinct as the RTA temperature increased. A continuous film of melted material  $500\text{--}700 \text{ nm}$  thick formed on the substrate surface when the temperature reached  $950^\circ\text{C}$ , which exceeded the melting point of Ge ( $938.2^\circ\text{C}$ ). Signs of the porous Si skeleton structure were already missing in this film. It was monolithic in the bulk with a few particles  $\sim 30\text{--}50 \text{ nm}$  in size on the surface.

An alloyed layer  $700\text{--}1000 \text{ nm}$  thick also formed on the substrate surface if the RTA duration was shortened by 10 times to 30 s. However, traces of the porous Si structure remained in the alloyed material.

EDX found that the obtained films consisted of Si and Ge with inclusions of O and C. The fraction of Ge in the film increased from 0.36 to 0.71 as the synthesis temperature increased from  $750^\circ\text{C}$  to  $950^\circ\text{C}$ . A small concentration of oxygen was present in the layer because of oxidation of inactive regions of the porous Si during electrochemical deposition of Ge in the heated aqueous electrolyte [20]. Organic compounds remaining in the porous Si matrix after electrochemical treatment could be an oxygen source in the formed alloy layer. Its concentration was rather high and reached 14–15 at.%.

Raman spectra of the samples also changed considerably as the RTA temperature increased. The sample annealed at  $750^\circ\text{C}$  showed two Raman lines (Fig. 3). The first with a maximum near  $521 \text{ cm}^{-1}$  corresponded to a triply degenerate optical vibrational mode of single-crystalline Si Si(LO) at the center of the Brillouin zone [21, 22]. The second at  $\sim 300 \text{ cm}^{-1}$  belonged to an analogous vibrational mode of crystalline Ge Ge(LO) [22].

Additional lines that corresponded to vibrations of Ge–Ge, Si–Ge, and Si–Si bonds in the crystalline  $\text{Si}_{1-x}\text{Ge}_x$  alloy appeared in the spectrum upon increasing the synthesis temperature to  $850^\circ\text{C}$  [23–26]. The lines had asymmetric shapes, indicating that low-dimensional effects, surface states, and defects or nonstoichiometric compositions arose in the material [27, 28]. Formation of the alloy was associated with a change of length and vibrational energy of bonds between Si and Ge atoms. Therefore, the positions of their maxima shifted from the fundamental values. Table 1 presents the positions of separate lines obtained by approximating the normalized Raman spectra of the samples by asymmetric sigmoidal functions.

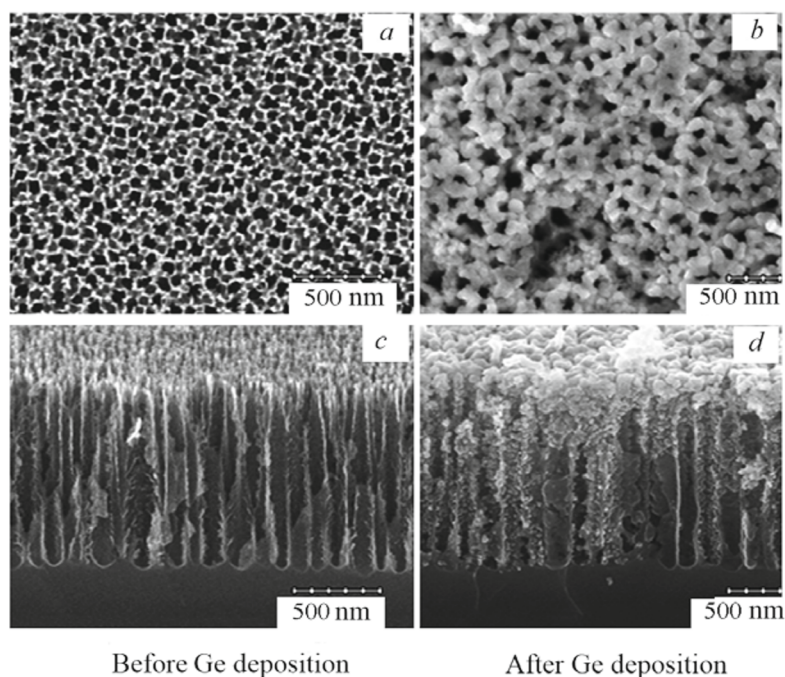


Fig. 1. Photomicrographs of the surface (a, b) and transverse chip (c, d) of porous silicon matrix before (a, c) and after (b, d) electrochemical deposition of germanium.

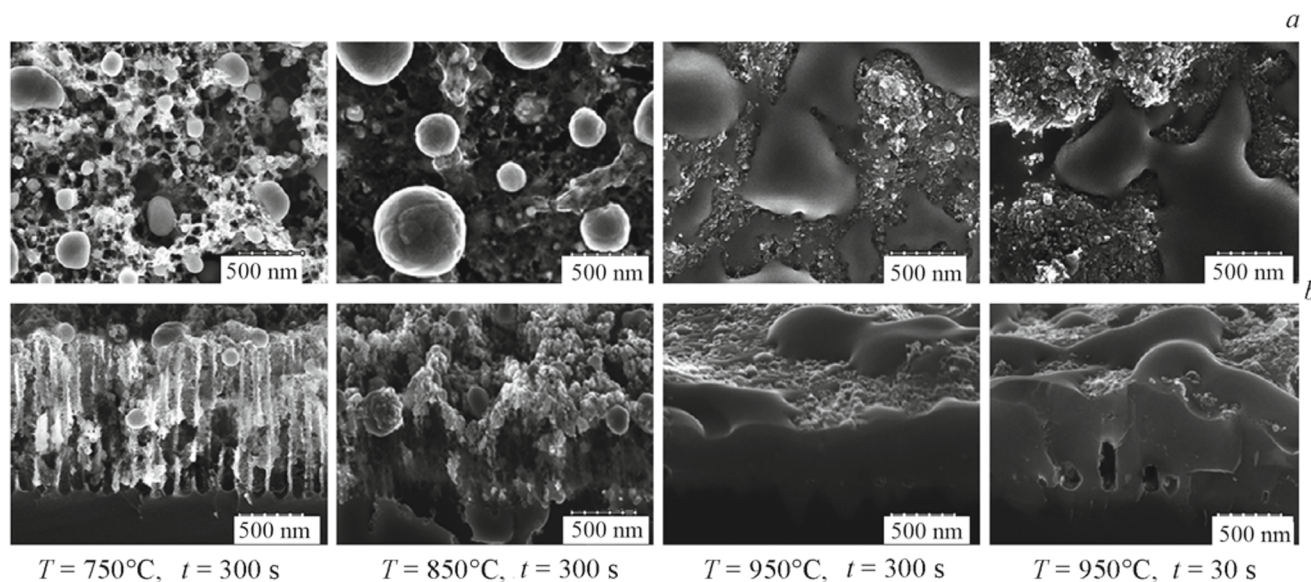


Fig. 2. Photomicrographs of the surface (a) and transverse chip (b) of porous silicon matrix with deposited germanium layer after 300 s of RTA at 750–950°C and after 30 s of RTA at 950°C.

The relative intensity of the SiGe Raman lines increased upon increasing the annealing temperature further to 950°C. The line with a maximum at  $521\text{ cm}^{-1}$  that corresponded to single-crystalline Si lattice vibrations weakened. The relative intensity of the line corresponding to vibrations of Si–Ge bonds in the Raman spectrum decreased if the RTA duration decreased.

The results indicated that thermal annealing at 750°C did not lead to formation of the SiGe alloy. The structural rearrangement of the deposited Ge film surface (Fig. 2) was related to the low wettability of the Si surface by Ge and

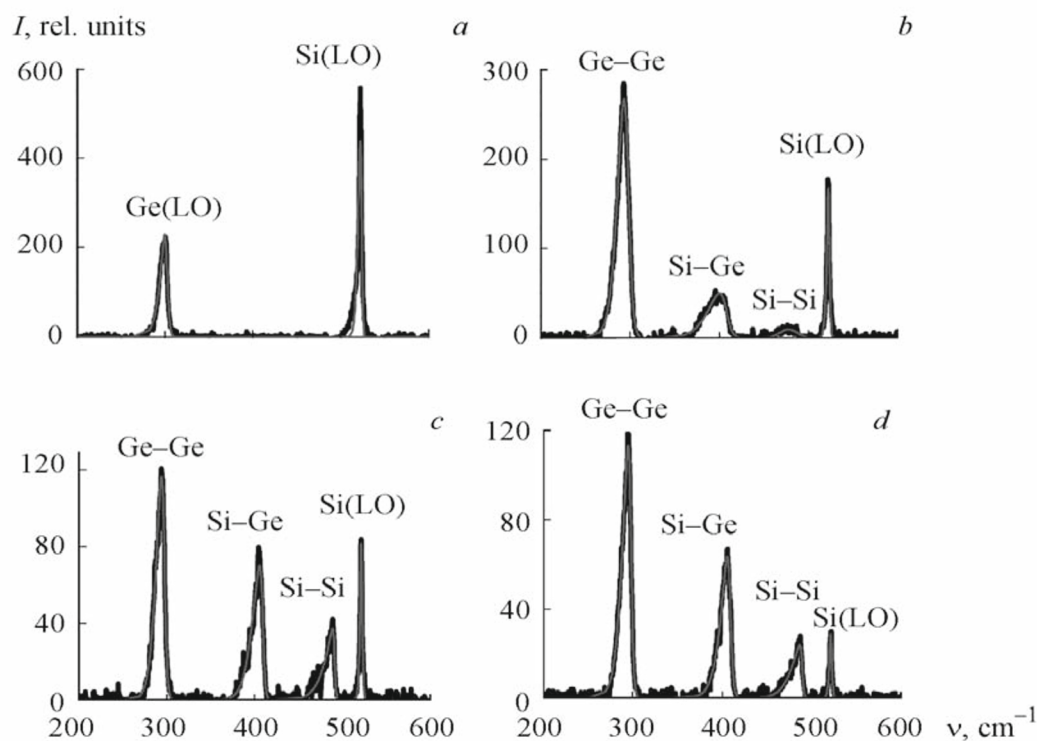


Fig. 3. Normalized Raman spectra of samples after RTA:  $T = 750^{\circ}\text{C}$ , process duration  $t = 300$  s (a),  $T = 850^{\circ}\text{C}$  and  $t = 300$  s (b),  $T = 950^{\circ}\text{C}$  and  $t = 300$  s (c),  $T = 950^{\circ}\text{C}$  and  $t = 30$  s (d).

TABLE 1. Parameters of Raman Spectra of  $\text{Si}_{1-x}\text{Ge}_x$  Alloy Samples Prepared at Various Temperatures and RTA Durations

RTA temperature, $^{\circ}\text{C}$	RTA duration, s	$\nu, \text{cm}^{-1}/I_{\text{norm}}, \text{rel. units}$		
		Ge-Ge	Si-Ge	Si-Si
850	300	292.7/1	404.3/0.19	488.9/0.04
950	300	293.8/1	404.3/0.60	488.9/0.32
950	30	294.4/1	406.1/0.56	487.1/0.21

mechanical stresses related to the misfit of the crystal lattices of the materials [23]. According to RS, SiGe films formed on the substrate surface if the temperature rose further to  $850^{\circ}\text{C}$ , despite the lack in the Si-Ge system of SiGe eutectic alloys with melting points less than that of Ge. The probabilities of forming Ge-Ge, Si-Ge, and Si-Si bonds were close to  $x^2$ ,  $2x(1-x)$ , and  $(1-x)^2$ , respectively, for a random distribution of Si and Ge atoms in the  $\text{Si}_{1-x}\text{Ge}_x$  alloy [24, 29]. The intensities of lines  $I$  (rel. units) in Raman spectra were proportional to the number of the corresponding chemical bonds. In this instance, the intensity ratio of Raman lines belonging to these bonds were [25, 29]:

$$I_{\text{Ge-Ge}}/I_{\text{Si-Ge}} = Bx/2(1-x), \quad (1)$$

$$I_{\text{Si-Si}}/I_{\text{Si-Ge}} = A(1-x)/2x. \quad (2)$$

Proportionality coefficients  $A$  and  $B$  were necessary to compensate for resonance effects leading to a dependence of the Raman line intensities on the excitation wavelength. The method for determining the Ge concentration from the intensity ratio of Raman lines did not depend on stresses in the alloy film. It was assumed that an excess of Ge was present in the obtained material so that the Raman line corresponding to Ge-Ge bonds included signals of both pure Ge crystallites and the alloy. However, the Si-Ge and Si-Si lines could belong only to the alloy. Therefore, the following fractions  $x$  of

Ge in the  $\text{Si}_{1-x}\text{Ge}_x$  alloy were obtained by using experimental coefficients  $A$  and  $B$  from the literature [29] and Eq. (2): for RTA duration 300 s and RTA temperature 850°C, 0.82; for 950°C, 0.63. Reducing the RTA duration to 30 s caused the Ge fraction to increase to 0.71. The calculated Ge concentrations in samples synthesized at 950°C were close to the EDX analytical results. EDX analytical results for samples synthesized at a lower temperature were indicative of a much lower concentration of Ge relative to Si (0.35–0.36). This was due to a feature of the EDX method that considered all atoms of materials located in the scanned region in both elemental semiconducting Si and Ge and the SiGe alloy. More accurate data on the material composition and structure could be obtained by using RS and recording the energy of bond vibrations between atoms of just the SiGe alloy.

Thus, the RS results for films of  $\text{Si}_{1-x}\text{Ge}_x$  alloy showed that Ge was distributed throughout a larger volume of the porous layer if the RTA temperature was increased and the RTA duration was unchanged. This was associated with a drop of its concentration in the formed alloy. Decreasing the annealing duration led to formation of  $\text{Si}_{1-x}\text{Ge}_x$  alloy films with a higher Ge concentration.

**Conclusions.** The RS study of thin films of  $\text{Si}_{1-x}\text{Ge}_x$  alloy obtained on single-crystalline Si substrates using electrochemical deposition of Ge onto a porous Si matrix followed by RTA showed that the composition and morphology of the formed alloy layer could be controlled by changing not only the process temperature but also its duration. It was found that the  $\text{Si}_{1-x}\text{Ge}_x$  alloy formed at an RTA temperature above 850°C. The fraction of Ge in the  $\text{Si}_{1-x}\text{Ge}_x$  alloy decreased from 0.82 to 0.63 upon increasing the RTA temperature from 850 to 950°C. This indicated that Ge was readily distributed throughout the porous Si matrix bulk containing many defects and surface states. A layer of  $\text{Si}_{1-x}\text{Ge}_x$  alloy with a greater Ge concentration formed if the RTA duration decreased from 300 to 30 s. The results for the ability to control the composition of the  $\text{Si}_{1-x}\text{Ge}_x$  alloy formed by the electrochemical method followed by RTA could be used to fabricate various devices based on SiGe for functional electronics, e.g., thermoelectric energy converters or optoelectronic devices.

**Acknowledgment.** The work was supported by a Russian Science Foundation Grant, Project No. 20-19-00720.

## REFERENCES

1. Y. Shiraki and N. Usami, *Silicon–Germanium (SiGe) Nanostructures: Production, Properties and Applications in Electronics*, Woodhead Publishing, Cambridge (2011), pp. 3–25.
2. L. Vegard, *Z. Phys.*, **5**, 17–26 (1920).
3. J. P. Dismukes, L. Ekstrom, and R. J. Pfaff, *J. Phys. Chem.*, **68**, 3021–3027 (1964).
4. N. M. Ravindra, B. Jariwala, A. Banobre, and A. Maske, *Thermoelectrics: Fundamentals, Materials Selection, Properties, and Performance*, Springer, Cham (2019), pp. 49–67.
5. V. I. Talanin, *New Research on Silicon — Structure, Properties, Technology*, IntechOpen, London (2017), pp. 84–101.
6. D. Benedikovic, L. Virost, G. Aubin, J.-M. Hartmann, F. Amar, X. Le Roux, C. Alonso-Ramos, E. Cassan, D. Marris-Morini, J.-M. Fedeli, F. Boeuf, B. Szlag, and L. Vivien, *Nanophotonics*, **10**, 1059–1079 (2021).
7. X. Zhang and L.-D. Zhao, *J. Materiomics*, **1**, 92–105 (2015).
8. I. M. Gavrilin, N. L. Grevtsov, A. V. Pavlikov, A. A. Dronov, E. B. Chubenko, V. P. Bondarenko, and S. A. Gavrilov, *Mater. Lett.*, **313**, Article ID 131802 (2022).
9. E. Fahrenkrug, J. Biehl, and S. Maldonado, *Chem. Mater.*, **27**, 3389–3396 (2015).
10. I. M. Gavrilin, D. G. Gromov, A. A. Dronov, S. V. Dubkov, R. L. Volkov, A. Yu. Trifonov, N. I. Borgardt, and S. A. Gavrilov, *Semiconductors*, **51**, 1067–1071 (2017).
11. S. Acharya, L. Ma, and S. Maldonado, *ACS Appl. Nano Mater.*, **1**, 5553–5561 (2018).
12. Q. Cheek, E. Fahrenkrug, S. Hlynchuk, D. H. Alsem, N. J. Salmon, and S. Maldonado, *ACS Nano*, **14**, 2869–2879 (2020).
13. R. Schwarz, F. Heinrich, and E. Hollstein, *Z. Anorg. Allg. Chem.*, **229**, 146 (1936).
14. C. G. Fink and V. M. Dokras, *J. Electrochem. Soc.*, **95**, 80–97 (1949).
15. N. Brinda-Konopik and G. Schade, *Electrochim. Acta*, **25**, 697–701 (1980).
16. R. K. Pandey, S. N. Sahu, and S. Chandra, *Handbook of Semiconductor Deposition*, Marcel Dekker Inc., New York (1996), pp. 201–203.
17. N. Chandrasekharan and S. C. Sevov, *J. Electrochem. Soc.*, **157**, C140–C145 (2010).
18. L. K. van Vugt, A. F. van Driel, R. W. Tjerkstra, L. Bechger, W. L. Vos, D. Vanmaekelbergh, and J. J. Kelly, *Chem. Commun.*, **2002**, 2054–2055 (2002).
19. E. B. Chubenko, S. V. Redko, A. I. Sherstnyov, V. A. Petrovich, D. A. Kotov, and V. P. Bondarenko, *Semiconductors*, **50**, 372–376 (2016).

20. K.-H. Li, C. Tsai, S. Shih, T. Hsu, D. L. Kwong, and J. C. Campbell, *J. Appl. Phys.*, **72**, 3816–3817 (1992).
21. I. P. Herman, *Optical Diagnostics for Thin Film Processing*, Academic Press, San Diego (1996), pp. 559–590.
22. J. H. Parker, D. W. Feldman, and M. Ashkin, *Phys. Rev.*, **155**, 712–714 (1967).
23. A. ShklyaeV, V. A. Volodin, M. Stoffel, H. Rinnert, and M. Vergnat, *J. Appl. Phys.*, **123**, Article ID 015304 (2018).
24. M. I. Alonso and K. Winer, *Phys. Rev. B: Condens. Matter*, **39**, 10056–10062 (1989).
25. P. M. Mooney, F. H. Dacol, J. C. Tsang, and J. O. Chu, *Appl. Phys. Lett.*, **62**, 2069–2071 (1993).
26. F. Pezzoli, E. Bonera, E. Grilli, M. Guzzi, S. Sanguinetti, D. Chrastina, G. Isella, H. von Kanel, E. Wintersberger, J. Stangl, and G. Bauer, *Mater. Sci. Semicond. Process.*, **11**, 279–284 (2008).
27. V. I. Korepanov and D. M. Sedlovets, *Analyst*, **143**, 2674–2679 (2018).
28. Y. Gao and P. Yin, *Sci. Rep.*, **7**, Article ID 43602 (2017).
29. S. A. Mala, L. Tsybeskov, D. J. Lockwood, X. Wu, and J.-M. Baribeau, *J. Appl. Phys.*, **116**, Article ID 014305 (2014).